# Enhanced 20th century heat transfer to the Arctic simulated in the context of climate variations over the last millennium

**J.H. Jungclaus, K. Lohmann, and D. Zanchettin**

{Max Planck Institut für Meteorologie, Hamburg, Germany}

Correspondence to: J. H. Jungclaus (johann.jungclaus@mpimet.mpg.de)

**Abstract**

Oceanic heat transport variations, carried by the northward flowing Atlantic Water, strongly influence Arctic sea-ice distribution, ocean-atmosphere exchanges, and pan-Arctic temperatures. Paleoceanographic reconstructions from marine sediments near Fram Strait have documented a dramatic increase in Atlantic Water temperatures over the 20th century, unprecedented in the last millennium. Here we present results from Earth system model simulations that reproduce and explain the reconstructed exceptional Atlantic Water warming in Fram Strait in the 20th century in the context of natural variability during the last millennium. The associated increase in ocean heat transfer to the Arctic can be traced back to changes in the ocean circulation in the sub-polar North Atlantic. An interplay between a weakening overturning circulation and a strengthening sub-polar gyre as a consequence of 20th century global warming is identified as driving mechanism for the pronounced warming along the Atlantic Water path toward the Arctic. Simulations covering the late Holocene provide a reference frame that allows us to conclude that the changes during the last century are unprecedented in the last 1150 years and that they cannot be explained by internal variability or natural forcing alone.

## 1 Introduction

The Arctic is one of the regions where climate change has been diagnosed most drastically in terms of warming and sea-ice decline over the last decades. Direct temperature measurements are, however, scarce and only available for the last century. Reliable observations of sea-ice evolution are even more limited, covering only the satellite era. On decadal timescales, internal variations can substantially contribute to Arctic climate variability (Bengtsson et al., 2004; Beitsch et al., 2014) and the relative role of external drivers is still under debate (Booth et al., 2012; Zhang et al., 2013). High-resolution reconstructions of paleoclimatic variables over the late Holocene provide a reference frame and put recent changes in context with long-term natural variations. Ongoing efforts, such as the Past Global Changes 2K network (PAGES2K, Ahmed et al. 2013) initiative, provide regional syntheses of reconstructions that can be compared with model simulations. While most of the PAGES2K reconstructions rely on terrestrial proxies, high-quality marine paleodata become increasingly available at annual to decadal resolution. Novel proxies have been developed to reconstruct, for example, dynamical quantities such as near-bottom flow strength in the Nordic Seas overflow regions (e.g., Mjell et al. 2014). Of particular value are reconstructions from key locations, such as major conduits of the large-scale ocean circulation. Spielhagen et al. (2011) and Dylmer et al. (2013) have published records from marine sediments off Svalbard that reflect temperature changes in the Atlantic Water (AW) in Fram Strait over the last 2000-3000 years. The time series show centennial-scale modulations of the AW temperatures and, as a pronounced common feature, a dramatic, unprecedented warming over the 20th century. The authors speculate that the observed warming reflect considerable changes in the lateral heat transfer to the Arctic that might have contributed to the rapid warming and sea-ice decrease during the 20th century.

Earth system model simulations over the last millennium provide a tool to test such hypotheses, and to investigate the relative role of internal variability on the one hand, and natural and anthropogenic forcing on the other hand. Provided that the model adequately simulates regional-scale features, simulations also allow for attributing locally observed variations to changes in large-scale dynamics.

52    In general, the model results have to be confronted with observations and reconstructions to assess

53    in how far they reproduce the real climate evolution, both in direct comparison (e.g., Fernandez-

54    Donado et al. 2012) and in a statistical sense (Bothe et al., 2013). In this paper, we use the results of

55    Max Planck Institute Earth System Model (MPI-ESM) simulations for the last millennium and the

56    industrial period to address the following research questions:

57        1.  Can the simulations reproduce important features of reconstructed climate indicators in high

58            northern latitudes during the last millennium and in the 20th century, both on a continental

59            and local scale?

60        2.  How exceptional is the observed 20th century AW warming in Fram Strait in the context of

61            the climate evolution during the last millennium, and what implications does it have for the

62            heat transfer to the Arctic?

63        3.  What are the mechanisms behind the observed and reconstructed changes?

64    Regarding the latter, we concentrate in this paper on the 20th century changes in high northern

65    latitudes and the North Atlantic and devote a subsequent study to pre-industrial variations and their

66    relation to external forcing. The paper is organized as follows. In section 2, we describe the MPI-ESM

67    model set-up and the boundary conditions applied for the simulations covering the last millennium.

68    Results for integrated high-northern latitude changes and the evolution of the Atlantic Water

69    transfer from the North Atlantic to the Arctic are given in section 3. In section 4, we formulate a

70    dynamical interpretation of the results and discuss implications for 20th century climate change in the

71    North Atlantic realm in section 5.  Main conclusions are given in section 6.

72

73    **2. The Model system and the experimental design of the last millennium simulations**

74    The model employed in this study is the Max Planck Institute Earth System Model (MPI-ESM). MPI-

75    ESM and its various configurations contributing to the Coupled Model Intercomparison Project,

76    phase 5 (CMIP5), have been documented in a special issue of the Journal for Advances in Modeling

77    Earth Systems (JAMES). The configuration for Paleo applications (MPI-ESM-P) used here is identical

78    with the MPI-ESM-LR configuration described in the JAMES publications by Giorgetta et al. (2013)

79    and Jungclaus et al. (2013) with two exceptions: First, the dynamic vegetation module is switched off

80    in order to allow for the implementation of land-cover change maps (Pongratz et al. 2008) as in the

81    earlier, lower-resolution model version described by Jungclaus et al. (2010). Second, the orbital

82    forcing is prescribed by a table providing annual values for eccentricity, obliquity and perihelion,

83    whereas the LR version uses a calendar-based orbit. The atmosphere model ECHAM6 (Stevens et al.

84    2013) is run at a horizontal resolution of spectral truncation T63 (1.875°) and 47 vertical levels,

85    resolving the stratosphere up to 0.01 hPa. The ocean/sea-ice model MPIOM (Marsland et al. 2003;

86    Jungclaus et al. 2013) features a conformal mapping grid with nominal 1.5° resolution and 40 vertical

87    levels (GR1.5L40). It is noteworthy for our study that the GR1.5L40 grid possesses one grid pole over

88    Antarctica and one grid pole over Greenland, which leads to considerably higher resolution in the

89    regions of interest for this study, i.e. the northern North Atlantic (Jungclaus et al. 2008). In Fram

90    Strait, for example, the grid size in cross-channel direction is about 30-40 km. The simulations over

91    the last millennium (past1000) follow the protocol of the Paleo Modeling Intercomparison Project,

92    phase 3 (PMIP3). As part of this protocol, Schmidt et al. (2011) summarize different choices for

93    external forcing and boundary conditions and provide tables for well mixed-greenhouse gases ($CO_2$,

94    $CH_4$, $N_2O$), and orbital parameters. In contrast to the millennium simulations described in Jungclaus

95    et al. (2010), which featured an interactive carbon-cycle and prognostic $CO_2$, we use prescribed $CO_2$

96    in the past1000 runs analyzeded here. We employed the Crowley and Unterman (2013)

97    reconstruction for volcanic aerosol optical depth and effective radius and the Pongratz et al. (2008)

98    reconstruction of global land-cover and agricultural areas. For solar radiation we have followed the

99    approach described in Schmidt et al. (2011) combining the Vieira et al. (2011) total solar irradiance

100   (TSI) reconstruction over the Holocene with the Wang et al. (2005) data set that provides the

101   recommended solar forcing for the CMIP5 20th century (1850 – 2005) simulations. An artificial 11-yr

102   cycle of varying amplitude is imposed over the pre-industrial period (see Schmidt et al., 2011 for

103   details). Linear interpolation was used to calculate monthly TSI averages from the reconstructed

104     annual TSI values for the period 850-1849 scaled to Total Irradiance Monitor (TIM) data, except for

105     the flux at 180.5 nm. Spectral Solar Irradiance (SSI) for the 14 short-wave spectral bands of the

106     ECHAM6's radiation scheme was calculated so that the sum of SSI yields TSI. Energy in the part of the

107     spectrum below the shortest wavelength of the radiation scheme (200nm) and above the longest

108     (12195.1 nm) was added to the first and last band, respectively. Monthly average ozone

109     concentrations for the period 850-1849 are calculated using the 1850-1860 monthly climatology of

110     ozone concentrations from the AC&C/SPARC Ozone Database as a basis and representing the ozone

111     dependency on solar irradiance through regression coefficients between historical ozone

112     concentrations and the annual 180.5 nm solar flux. An 1155 year-long pre-industrial control

113     integration (PiCtrl) under fixed 1850 boundary conditions serves as a reference simulation for forced

114     experiments. To conduct the past1000 simulations we first ran a 400 year-long adaptation simulation

115     starting from the end of piCtrl to adjust to 850 boundary conditions and thereafter started the three

116     realizations past1000-r1, past1000-r2, and past1000-r3. The past1000-r1 and past1000-r2

117     experiments were initialized with the same ocean state, but differ in the standard deviation of the

118     assumed lognormal distribution of the volcanic aerosol size (1.2 µm in r1, 1.8 µm in r2 and r3). The

119     simulations past1000-r2 and past1000-r3 used the same parameter setting but were started from

120     different initial conditions. Furthermore, ozone concentration data used in past1000-r1 are affected

121     by use of a 1-month-shifted annual cycle in the AC&C/SPARC ozone climatology, an issue solved in

122     past1000-r2 and –r3. While the three simulations are therefore not an ensemble of three runs

123     carried out with an identical model and forcing/boundary conditions, we consider the effect of the

124     different setting small enough to regard the runs as three realizations of possible last millennium

125     climate evolution under parameter and forcing uncertainties. The PMIP3 protocol defines the

126     past1000 integration period as 850-1849. To relate the recent climate evolution to the late-Holocene

127     variability we continued the respective past1000 simulations over the historical period (1850 – 2005).

128     The applied boundary conditions follow the CMIP5 protocol, except for land-cover-changes where

129     we continue the simulations with the Pongratz et al. (2008) data set. In the following, we refer to the

130 combined past1000 and historical simulations covering the period 850-2005 as pr1, pr2, and pr3,

131 respectively. Since the emphasis of our present study is on the 20th century changes, we also include

132 in some analyses in section 4 and 5 one additional "historical" (hr1) simulation (1850-2005), which

133 was initialized from the PiCtrl experiment.

134

## 3. Last millennium evolution of high northern latitude climate

### 3.1 Pan-Arctic temperature and sea-ice extent

137 We start the analyses with quantities that reflect the general climate evolution in high northern

138 latitudes. Reconstructing regional-scale temperature and other climate variables such as sea-ice

139 extent in sparsely-sampled areas is still challenging. Only recently pan-Arctic reconstructions for

140 temperature have been published (Kaufman et al., 2009; Shi et al. 2012), mostly based on terrestrial

141 proxies (tree-rings) and ice cores. The PAGES2K consortium reviewed reconstruction data and

142 methods and constructed seven continental-scale temperature records, including the Arctic (Ahmed

143 et al. 2013). The reconstructed temperature records (black lines in Figure 1 a) have in common that

144 they show a gradual cooling during the last millennium, possibly reflecting the overall evolution from

145 a warmer Medieval Warm Period (MWP) to an anomalously cold Little Ice Age (LIA). Note that the

146 PAGES2K record reflects annual mea temperatures whereas the other two represent the summer

147 season. All reconstructions (and the instrumental data that they are matched to) show a strongly

148 reversed trend during the 20th century. The Shi et al. (2012) and Kaufman et al. (2009) summer

149 temperature reconstructions disagree on the magnitude of the pre-industrial cooling. This reflects

150 differences in the proxies chosen, their geographical distribution, and the statistical methods used to

151 match the proxies to historical observations. We are not in a position to judge which of the two time

152 series reflects more appropriate the real climate evolution; we therefore regard the discrepancy as a

153 measure of uncertainty in reconstructed climate. The simulated summer temperatures are

154 compatible with the reconstructions and match closely the Kaufman et al. (2009) data. Individual

155 simulations (colored lines in Figure 1 a) show relatively strong fluctuations and ensemble realizations

156   differ often quite strongly (about 0.5°C) for a given period. In contrast to global and hemispheric

157   averages (not shown here, but see Figure 5 in Jungclaus et al. 2010), individual volcanic eruptions

158   (like the very strong 1258 or 1453 tropical eruption) or clusters of volcanic events are not clearly

159   discernible, with the exception of the 1809 and 1815 (Tambora) eruptions, where all simulations

160   show a similar cold excursion, in accordance with the Kaufman and Past2K reconstructions. The

161   resilience to volcanic forcing reflects the relatively small signal-to-noise ratio of Arctic summer

162   temperatures, due to both strong internal variability of the Arctic regional climate (e.g. Beitsch et al.,

163   2014) and seasonal character of local response mechanisms, which are most prominent in boreal

164   winter (e.g., Zanchettin et al., 2012). Zanchettin et al. (2013) have also highlighted the role of

165   background conditions (e.g. during the closely following 1809 and 1815 eruptions) for the actual

166   response pattern in particular at high latitudes.

167   The Arctic warming throughout the 20th century is also well reflected in the model simulations and

168   the pronounced variations such as the warm phase in the first half of the last century are well within

169   the ensemble range of the historical experiments.

170   The summer sea-ice reconstruction by Kinnard et al. (2011) comes with a relatively large range of

171   uncertainty (dashed black lines in Fig. 1b) but the main characteristic is that of a mirror-image of the

172   pan-Arctic surface temperature evolution: A gradual increase in sea-ice extent during the pre-

173   industrial millennium is replaced by a drastic decline in the 20th century (Figure 1 b). The decline of

174   sea-ice extent sets in, however, more abruptly in the mid-20th century in contrast to the relatively

175   gradual warming. The past1000 simulations reproduce a similar long-term trend over the pre-

176   industrial millennium and the 20th century simulations terminate at an extent that is equally low as

177   the observations. In the simulations, the sea-ice decline begins, however, earlier featuring a temporal

178   evolution more similar to the pan-Arctic temperature (Figure 1a). In fact, all four historical

179   simulations show ice extent anomalies below the reconstruction's mean estimate between 1870 and

180   1950. The sea-ice reconstruction exhibits a pronounced relative minimum in the late 16th century,

181   which none of the three past1000 simulations reproduces. Notwithstanding questions regarding

182 uncertainties in the reconstructions, it is difficult to relate the event to known volcanic or solar

183 forcing variations (e.g. the minimum around 1700 appears at the time of the Maunder minimum in

184 solar variations). The anomalies in the 15th to 17th century exceed the 2-sigma range of control

185 experiment variability significantly. We have detected events of similar magnitude in unforced

186 control simulations, but they appear only very rarely (once in a 1000 yr simulation). It is therefore

187 possible that the model underestimates internal variability of the sea-ice extent.

188

189 **3.2 Fram Strait Atlantic Water temperatures**

190 The reconstructions of AW temperatures stem from a marine core at site MSM5/5-712 at

191 78°54.94'N, 6°46.04'E (see Spielhagen et al. (2011) and Werner et al. (2011) for details). The authors

192 provide two temperature records, one based on a modern analogue technique (SIMMAX), and one

193 based on the Magnesium-Calcium (Mg/Ca) ratio of *Neogloboquadrina pachyderma*. Habitat and

194 plankton bloom estimates indicate that both proxies reflect mid-summer conditions in the upper part

195 of the AW layer. During pre-industrial times, the Mg/Ca-derived record exhibits much stronger

196 variability, which might reflect inaccuracies in recording the cold-water range (Spielhagen et al.,

197 2011). Both reconstructions, however, fluctuate around very similar pre-industrial mean values (3.4°

198 and 3.6°C) and indicate a warming of roughly 2°C during the 20th century (Figure 2). A similar

199 temperature increase is also found in continued measurements from Svalbard fjords from 1912 to

200 2005 (Pavlov et al., 2013) and agrees with previous estimates of 20th century evolution of AW

201 properties in the northern North Atlantic (Polyakov et al., 2004). Another late-Holocene sedimentary

202 record from Malangen Fjord in northern Norway (Hald et al. 2011) reflects local variations in the

203 influx of AW and shows a similar temperature evolution over the last 1200 years including an

204 unprecedented warming in modern times.

205 We compare the Spielhagen et al. (2011) reconstructions with simulated fluctuations of

206 temperatures in the AW core at 50m depth in Fram Strait at about 78°N (Figure 2). The relatively low

207 temporal resolution and the strong fluctuations in the Mg/Ca record prohibit a very detailed

208    comparison in the pre-industrial millennium. The simulations and the SIMMAX data agree in a change

209    from slightly warmer-than-average temperatures in the first centuries and colder conditions in the

210    16th to 18th centuries, reflecting the general change from MWP to LIA conditions. Interestingly, all

211    time-series show a cold spell in the early 19th century, likely recording the 1809 and 1815 eruptions.

212    During the 20th century, simulations and the SIMMAX record agree in a 2°C warming. The simulations

213    also exhibit considerable decadal to multidecadal variations that are not covered or sub-sampled by

214    the reconstructions' resolution. The ensemble spread and the relatively large variability range

215    obtained from the unforced control run (Figure 2), points to a large fraction of internal variability.

216    Clearly, the warming in the industrial period exceeds the 2σ-range of the undisturbed simulation.

217    Spielhagen et al. (2011) speculate that the diagnosed warming infers a considerable increase in heat

218    transfer to the Arctic. In the model simulations, we can quantify the heat flux changes and display in

219    Figure 3a the combined total ocean heat transport (TOHTR) through Fram Strait and through the

220    Barents Sea Opening (BSO), which both show the unprecedented increase in the 20th century. Firstly,

221    we confirm that the AW temperature record reflects indeed changes in heat transfer through the

222    most important conduits towards the Arctic. The correlation coefficients between AW temperatures

223    and TOHTR (smoothed by a 31-yr running mean) exceed 0.9 at zero time-lag in all three past1000

224    simulations. Simulated TOHTR anomalies are shown with respect to (w.r.t.) the pre-industrial (850-

225    1849) mean of about 80 TW (1 TW = $10^{12}$Watt). The simulated transports are compatible with

226    observations indicating a heat transport of 30-40 TW in Fram Strait (Schauer et al. 2008) and 30-76

227    TW in BSO (Årthun et al. 2012). Observations of heat transports are, however, only available for the

228    most recent decades and may be influenced by decadal-scale variability as well. During the pre-

229    industrial period, there are TOHTR fluctuations of the order of 10-20 TW and the ensemble indicates

230    somewhat higher-than-normal TOHTR in the early part of the simulation and less TOHTR in the 16th

231    and 17th century. Large volcanic eruptions (1258, 1453, and 1815) leave an imprint on the heat

232    transports leading to reduction of heat transfer to the Arctic (Zanchettin et al., 2012). The most

233    pronounced feature of our smoothed time series from the simulations is, however, a consistent

234 increase of up to 30 TW during the 20th century, reflecting a 40% increase over the pre-industrial

235 mean.

236 The modulation of the AW temperature could either be driven by local changes in the wind system

237 (Bengtsson et al. 2004) or be part of variations in the warm water path associated with the North

238 Atlantic Current or the Atlantic Meridional Overturning Circulation (AMOC), as has been suggested,

239 for example by Polyakov et al. (2004). However, recently Lozier (2010) and Lozier et al. (2010) have

240 demonstrated that overturning and gyre circulation in the North Atlantic are strongly linked and that

241 the image of a continuous conveyor belt associated with the AMOC may be misleading. Building on

242 earlier results analyzing Arctic warming events in an unperturbed control integration (Beitsch et al.,

243 2014) we therefore decompose the (TOHTR) in the Atlantic basin into its overturning and gyre

244 components (MOHTR, and GOHTR, respectively). The first reflects the zonal average heat transport,

245 the second the deviations of the zonal average (e.g. Eden and Jung, 2001; Drijfhout and Hazeleger,

246 2006). First, we calculate the correlations between the TOHTR at the entrance to the Arctic (Figure

247 3a) and the components of the basin-scale OHTRs for all latitudes. High correlations are found in

248 particular in the sub-polar North Atlantic between GOHTR and heat transfer to the Arctic (not

249 shown). At the entrance to the Nordic Seas at 60°-65°N (Figure 3b) we can see that most of the

250 modulation in the heat transfer to the Artic during the millennium can be traced back to downstream

251 fluctuations in GOHTR. The gyre heat transport features multi-centennial changes from stronger-

252 than-normal conditions in the early centuries of the simulation to weaker conditions during the Little

253 Ice Age. The 20th century stands out again with its unprecedented increase in the TOHTR. Most of the

254 increase at 60-65°N is carried by an increase in the gyre component, but, interestingly, also the

255 overturning component shows a clear positive trend over the 20th century and apparently

256 contributes to high-latitude warming despite the fact that AMOC is decreasing at 30°N over the 20th

257 century.

258

259 **4. Origin of the 20th century heat transfer increase**

260    In the following, we focus on the changes in the 20th century and elucidate the relation between heat

261    transfer changes in Fram Strait and the sub-polar North Atlantic. We consider simulated linear 100yr

262    trends (1905-2005) and compare them with the expected range of internal variability as expressed in

263    the 5-95%-tile range of the respective variables taken from the 1000 yr-long PiCtrl simulation.

264    The changes in the heat transport components over the 20th century reflect trends in the large-scale

265    ocean circulation. Figure 4 shows the centennial trends for the AMOC streamfunction (Figure 4a) as

266    function of latitude and the for the barotropic horizontal streamfunction (Figure 4b) together with

267    their long-term means. The AMOC increases at higher-latitudes, but the most prominent feature is a

268    broad-scale weakening in subtropical and subpolar latitudes at depth below 1000m. As has been

269    described in previous studies (e.g. Latif et al., 2006), this weakening is associated with reduced deep-

270    water formation, most prominently in the Labrador Sea (see below). On the other hand, the

271    circulation cell reaching into the Nordic Seas strengthens as more overturning occurs at higher

272    latitudes. The barotropic streamfunction trends are characterized mainly by a pronounced

273    strengthening (the negative sign refers to more cyclonic circulation) in the central and eastern part of

274    the subpolar basin. In the central Labrador Sea, the gyre circulation weakens, which is, again,

275    compatible with reduced deep water formation in the main convection region. There is also

276    indication of a weakening of the gyre circulation in the Nordic Seas.

277    The change in TOHTR in the Atlantic basin reflects the trends in its components: in particular in sub-

278    polar latitudes, a weaker overturning component is mostly compensated by a stronger gyre

279    component (Figure 5a), but the resulting TOHTR does not exceed the range of internal variability.

280    North of 55°N changes in both components are much smaller, but are constructively adding up to

281    positive TOHTR trends. The trends are robust in the four simulations, and the 20th century TOHTR

282    trends exceed the 5-95% range deduced from the PiCtrl run in three of the four simulations. In

283    subtropical latitudes, overturning transports are also smaller, but not compensated by the gyre

284    transports. Thus the TOHTR here are considerably weaker and exceed the 5-95%-tile range of trends

285    in the control simulation. Meridional divergence or convergence of TOHTR then causes regional

286  cooling or warming, if not compensated by surface heat fluxes. Therefore, positive slopes of the

287  TOHTR curves in Fig. 5a indicate cooling while negative slope indicate warming, as indicated by the

288  red and light-blue horizontal lines at the bottom of Figure 5a. Regions, where divergence of advective

289  lateral heat transport cools the ocean (Figure 5a) are associated with positive atmosphere-ocean

290  heat flux trends, indicating that the colder ocean is cooling the atmosphere. Hence the atmosphere is

291  damping the ocean-induced changes rather than enforcing them. Trends in the upper-ocean

292  temperatures are negative roughly between 45° and 60°N and, since they are only partly

293  compensated by freshening (not shown), there are considerable changes in the density structure as

294  is shown for the pr2 experiment in Figure 6 (results are similar for all simulations). Increased density

295  in the center and more pronounced doming of the subpolar isopycnals is typical for a strengthening

296  gyre. The increasing horizontal density gradients, on the other hand, indicate higher baroclinic

297  pressure gradients and further accelerate the gyre (Greatbatch et al., 1991; Levermann and Born,

298  2007).

299  A possible reason for the acceleration of the gyre circulation could be changes in the wind system.

300  Modulations of large-scale atmospheric pressure patterns like the North Atlantic Oscillation or the

301  East Atlantic Pattern leave their specific imprint on the wind-driven ocean circulation (Häkkinen and

302  Rhines, 2009) and may be important also on centennial time scales (e.g., Sedláček and Mysak, 2009).

303  In particular, the gyre would respond to changes in the wind-stress curl caused, for example, by a

304  poleward shift of the westerlies due to global warming (e.g. Saenko et al., 2005). The centennial

305  trends in the zonal wind stress component are indeed relatively coherent in the past1000

306  experiments and resemble those obtained by Saenko et al. (2005) in idealized $CO_2$-doubling

307  experiments: stronger positive wind stress north of 40°N and slightly negative values in the sub-

308  tropical region (Figure 7a). While consistent in three of the four experiments considered here, the

309  changes are well within the 5-95%tile range obtained from the unperturbed control experiment.

310  Moreover, trends in wind-stress curl (Figure 7b) indicate coherent changes only in the Southern

311    Hemisphere (not shown), which is, again, consistent with the findings by Saenko et al. (2005), who

312    applied somewhat stronger $CO_2$ forcing.

313    To further elucidate the origin of the circulation changes we identify first the reason for the

314    weakening of the AMOC in the subtropical and subpolar North Atlantic. A key ingredient modulating

315    the AMOC here is the strength of deep water formation in the Labrador Sea (Latif et al., (2006),

316    Lohmann et al., 2014). To quantify the latter we calculate the thickness of the Labrador Sea Water

317    (LSW) in the region (Lohmann et al., 2014). Normalizing the anomalies, we see a clear co-variability

318    with the AMOC at 30N and 1500m depth when AMOC lags by roughly 8-10 years. Next, we establish

319    a link between LSW thickness and surface properties by correlating LSW thickness with the surface

320    density field (not shown), which reveals the central Labrador Sea as convection hot-spot. The

321    evolution of surface density, temperature and salinity in the so-identified region reveals, as expected,

322    that enhanced LSW formation comes together with positive density anomalies at the surface, which

323    reduce the static stability and induce convection. Also shown in Figure 8a are the corresponding

324    temperature and salinity time series. Following the evolution through the last three centuries

325    indicate pronounced multi-decadal variability and pronounced differences between the industrial

326    period and the centuries before. The multidecadal variability is characterized by co-varying

327    temperature and salinity, where apparently, density is determined by the salinity changes (e.g.,

328    fresher and lighter conditions lead to less dense surface waters, which is not compensated by colder

329    temperatures). The variations in the regional fresh-water budget is mainly caused by modulations of

330    the sea-ice and fresh water supply from higher latitudes (Jungclaus et al., 2005). During the 20th

331    century, however, this relation breaks down as somewhat fresher conditions (also caused by

332    increasing sea-ice and fresh-water export through Denmark Strait, not shown) go along with a

333    general warming, partly caused by direct radiative forcing, partly be redistribution of heat by an

334    enhanced Irminger Current. As a result, AMOC weakens at latitudes downstream from the LSW

335    formation region. The temporal evolution of the vertical density structure in the Labrador Sea

336    indicates then generally less dense conditions in the upper 2000m. Interestingly, the deepest layers

337　are characterized by relatively colder temperatures and higher densities that are caused by the

338　enhanced overturning in the Nordic Seas and associated changes in the strength and density of the

339　Denmark Strait overflow. Changes in the vertical density structure are important for the east-west

340　density gradient driving the AMOC (Lozier et al., 2010), but also affect the baroclinic structure of the

341　gyre directly (Drijfhout and Hazeleger, 2006).

342

343　**5. Discussion**

344　Our analysis has demonstrated that the increasing heat transports to higher latitudes are mainly

345　caused by changes in the gyre and overturning circulation in the subpolar North Atlantic. These

346　changes are caused by a reduction in deep water formation in the Labrador Sea, which leads to

347　reduced overturning circulation in subtropical and subpolar latitudes. In addition, changes in the

348　vertical structure of water masses at the western boundary can modify the baroclinic gyre circulation

349　(Drijfhout and Hazeleger, 2006). The associated changes in MOHTR and GOHTR lead to enhanced

350　TOHTR towards higher latitudes and heat transport divergence (cooling) in the subpolar region. The

351　colder and denser SPG then spins up baroclinically, which further increases the GOHTR (dashed lines

352　in Figure 5a), which, in turn, extracts even more heat from the SPG center and further increases the

353　horizontal density gradient. Thus a positive feedback mechanism is initiated. The mechanism can be

354　compared to the one described by Levermann and Born (2007) and Born et al. (2013a). These

355　authors describe a positive feedback, where an (somehow) accelerated gyre leads to increasing east-

356　west temperature and salt transports along its northern rim. Increasing salinity then leads to denser

357　surface waters in the Labrador Sea and to enhanced convective activity, which further spins up the

358　gyre. In our simulations, we see also a redistribution of salinity during the 20$^{th}$ century change in gyre

359　circulation resulting in higher salinities in the western part of the basin. However, in contrast to the

360　mechanism described by Levermann and Born (2007), the positive temperature anomalies dominate

361　the near-surface density evolution and Labrador Sea convection rather decreases.  Levermann and

362　Born (2007) demonstrated that a bistability regime exists, where the transition between the two

363    regimes can be triggered by small fluctuations in surface freshwater flux. Born et al. (2013a)

364    extended the study and found multiple circulation modes in PiCtrl experiments in six out of 19

365    models (among them MPI-ESM-LR). Even though we find some differences to their mechanism, it is

366    possible that the relatively strong response of the SPG is an expression of such a transition, here

367    triggered by changes in the AMOC. Possibly also the wind-stress changes (Figure 7) play a role in

368    initiating the change in the gyre circulation by modified Ekman and/or Sverdrup transports.

369    Furthermore, gyre circulation changes can also directly be driven by changes in the baroclinic

370    structure at the western boundary as has been shown in the global warming simulations by Drijfhout

371    and Hazeleger (2006). At the western boundary near the exit of the Labrador Sea (Figure 8b), the

372    density changes are consistent with a weakening of Labrador Sea Water production and an increase

373    in overflow-derived density, similar to what has been found by Drijfhout and Hazeleger (2006). It is

374    difficult, however, to exactly detect which component is more important. For this, additional

375    sensitivity experiments (e.g., partial-coupling experiments) would be necessary, which is beyond the

376    scope of this study. In any case, an important ingredient is the weakening of the AMOC in subtropical

377    and subpolar latitudes, caused by a decrease in Labrador Sea Water formation as a response to

378    global warming, while the deep water production in the Nordic Seas is even slightly enhanced. The

379    exact mechanisms of how gyre and overturning circulations interact are also difficult to disentangle.

380    In the historical simulations, changes in AMOC and SPG circulation appear to happen more or less

381    instantaneous, whereas analyses of the unperturbed control simulation suggest that AMOC

382    variations are leading by a few years.

383    Many CMIP5 models feature a reduction of the AMOC strength already in the 20th century (Drijfhout

384    et al., 2012). A characteristic feature of these simulations is the "warming hole" above the sub-polar

385    North Atlantic that can also be identified in observations (e.g. in the HadSST data set; Rayner et al.,

386    2006). A cool surface temperature spot within the intensified SPG is also characteristic for our 20th

387    century simulations (Figure 3c) and clearly related to the mechanism described above. Drijfhout et al.

388    (2012) decompose the temperature pattern in a radiatively forced and an AMOC fingerprint and

389    conclude that the cold sub-polar North Atlantic is indeed related to an AMOC decline. Kim and An

390    (2012) come to a similar conclusion analyzing $CO_2$-doubling experiments from the Coupled Model

391    Intercomparison Project Phase 3 data base.

392    Another indication that the mechanism described here is at work in reality comes from

393    paleoceanographic reconstructions for the late Holocene. Miettinen et al. (2012) compare the

394    temporal evolution of ocean temperatures at two locations, the Voering Plateu in the Norwegian Sea

395    and the SPG region south of the Reykjanes Ridge. They find that low-frequency fluctuations occur

396    out-of-phase: the Voering Plateau record features, for example, a cold anomaly during the Little Ice

397    Age (LIA), whereas the SPG is warmer than normal during this period. Such a behavior is compatible

398    with the findings described here: A weaker SPG in the LIA (Figure 3) would feature a less dense and

399    warmer center (opposite to what is seen for the strong-gyre anomaly in Figure 6) and would

400    transport less heat to the Nordic Seas. Such out-of-phase anomalies of the barotropic stream

401    function in the SPG region and the Nordic Seas can also be seen in Figure 4b. A detailed investigation

402    of the variations and processes during the pre-industrial millennium and their relation to natural

403    forcing will be subject of a subsequent study.

404    Obtaining a comprehensive view from long-term direct observations of temperature, salinity, or

405    transports remains challenging. There exist only a few long-term time series. Many continuous

406    records, such as those from weather ships (e.g. Østerhus and Gammelsrød, 1999) cover the last

407    decades and are characterized by multi-decadal variability. The temperature measurements over the

408    $20^{th}$ century near Svalbard by Pavlov et al. (2013) and one of the longest time-series available at all,

409    the Kola section in the Barents Sea (Skagseth et al., 2008) support the pronounced warming in the

410    Atlantic Water branch in the industrial period. Polyakov et al. (2004) synthesized various

411    observational data sets to conclude that the intermediate Atlantic Water layer in the Arctic shows a

412    continuous warming trend that is superposed by multi-decal variability. Combining proxy data and

413    observations, Cunningham et al. (2013) compiled a synthesis of SST changes in the north-eastern

414    North Atlantic and the Nordic Seas during the last millennium. For the $20^{th}$ century (their Figure 1a),

415    they report that most of the records reflecting the Atlantic Water branch along Scotland and Norway

416    indicates a warming, while other records from the sub-polar North Atlantic indicate neutral or

417    cooling conditions. High-resolution proxies from the Iceland Basin (Hall et al., 2010) over the last 230

418    years indicate cooling of SSTs in the central subpolar gyre region, which would be consistent with our

419    findings. The available SST gridded data sets HadISST (Rayner et al., 2006) and ERSSTv3 (Smith and

420    Reynolds, 2004) as well as the Simple Ocean Data Assimilation (SODA) reanalysis (Carton and Giese,

421    2008) are all characterized by a cooling trend in the subpolar gyre region (Drijfhout et al., 2012; Kim

422    and An, 2012). Polyakov et al. (2010) have used historical data from the North Atlantic Ocean and

423    decomposed the changes between the 1920s and present into non-linear trend and multi-decadal

424    variability patterns. The large-scale nonlinear trend pattern resembles the 20$^{th}$ century SST trend in

425    the HadISST and is characterized by cooling over the subpolar gyre (see their figure 5) and warming in

426    the subtropical North Atlantic and on the northwestern European Shelf, again compatible with our

427    results for the 20$^{th}$ century simulations. On the other hand, the 20$^{th}$ century compilation of

428    temperature and salinity data from the subpolar gyre region by Reverdin (2010) compares less well

429    with our study: the central SPG at about 60N is characterized by slightly positive temperature and

430    negative density trends.

431    Uncertainties in early observations and reconstructions preclude a definite answer to what degree

432    the findings reported here can be verified by observations. While the dynamical mechanisms

433    proposed here to explain the enhanced heat transfer to the Arctic appear largely compatible with

434    observed features in the North Atlantic, they may depend on the particular model system. Moreover,

435    as many other CMIP5 models, MPI-ESM features large SST and circulation biases in the North

436    Atlantic. In particular, the path of the Gulf Stream/North Atlantic Current is too zonal (Jungclaus et

437    al., 2013), which has direct consequences for the shape of the gyres. This may affect the warm water

438    path from the Subtropics to the Nordic Seas. Using observations and model simulations for the

439    second half of the 20$^{th}$ century, Hatún et al. (2005) concluded that a weaker (and less zonally-

440    extended) SPG would allow more warm and saline water to enter the Nordic Seas. Our simulations,

441    but also other CMIP5 ESMs (Born et al., 2013a; Koenigk and Bradeau, 2014) and stand-alone ocean

442    model simulations with the same ocean model as used here, but forced by reanalysis data (Müller et

443    al., 2014) suggest that a stronger SPG carries more subtropical AW into the Nordic Seas and the

444    Arctic. This discrepancy may be related to the specific situation of the late 20th century described by

445    Hatún et al. (2005), where SPG changes were mainly related to the atmospheric forcing (Häkkinen

446    and Rhines, 2009; see also Born et al., 2013b).

447    A 30 TW increase in heat transfer to the Arctic over 100 years as suggested by our simulations for the

448    20th century is an important contribution to the Arctic heat budget (Serreze et al., 2007). Dividing by

449    the area of the Arctic, it corresponds to a substantial forcing of about 2 $Wm^{-2}$. Jungclaus and Koenigk

450    (2010) and Beitsch et al. (2014) have shown that multidecadal variations in TOHTR to the Arctic

451    impact the Arctic climate. For positive TOHTR anomalies, the sea-ice cover decreases most

452    pronounced in the Barents Sea and causes considerable variations in ocean-atmosphere heat fluxes.

453    Although only a small fraction of the Arctic is affected, the associated warming leads to positive pan-

454    Arctic temperature anomalies. Moreover, the heat-flux changes affect the atmospheric circulation.

455    An associated feedback mechanism is the Bjerknes Compensation (Bjerknes, 1964; Shaffrey and

456    Sutton, 2006; Jungclaus and Koenigk, 2010): on multidecadal time-scales, TOHTR and atmospheric

457    heat transports (AHTR, here derived from the components of moist and dry static energy advection

458    following Keith (1995)) are strongly coupled and may compensate each other. Thus, both TOHTR and

459    AHTR need to be considered for an assessment of the lateral heat transfer changes as part of the

460    Arctic heat budget. Comparing TOHTR and AHTR at 70°N (Figure 7) indicates considerable

461    multidecadal variability where the respective TOHTR and AHTR tend to evolve out-of-phase.

462    However, there is no compensation of the strong positive trend in TOHTR during the last decades of

463    the simulation. Therefore we conclude that there is a net positive contribution from the lateral heat

464    fluxes to the Arctic heat budget and to the warming in recent decades. An assessment of all terms of

465    the Arctic heat budget and the feedback mechanisms leading to Arctic Amplification is, however,

466    beyond the scope of our paper. The magnitude of TOHTR changes appears to play a decisive role in

467 the amplitude of pan-Arctic warming, and sea-ice evolution in climate-change simulations (Mahlstein

468 and Knutti, 2011). These authors concluded that the TOHTR changes contribute significantly to Arctic

469 amplification, but they also identified considerable differences in the TOHTR magnitude in the

470 CMIP3-model suite as a cause for model uncertainty in projected Arctic warming.

471

472 **6. Conclusions**

473 The MPI-ESM last-millennium simulations consistently reproduce enhanced 20th century warming of

474 AW at the boundary between the Nordic Seas and the Arctic compared with pre-industrial variability.

475 The warming of AW in Fram Strait is an indicator for a prominent (~40%) increase in oceanic heat

476 transfer to the Arctic during the 20th century. In the simulations, we are able to trace back the heat

477 transport changes to a reorganization of the large-scale ocean circulation in the sub-polar North

478 Atlantic. The SPG and the associated northward heat transport are intensified by the global-warming-

479 induced weakening of the AMOC and changes in the density structure associated with modified deep

480 water formation. The latter also lead to a slight intensification of the overturning in high northern

481 latitudes. Together, the gyre and overturning-related heat transport changes lead to an increase in

482 the heat transfer to the Nordic Seas and the Arctic. Changes in wind-stress curl do not appear to be

483 significantly different from the unperturbed variability, but wind-stress changes may nonetheless

484 play a role in triggering the mechanism. Transient simulations over the late Holocene provide a

485 valuable reference frame to discriminate unprecedented changes such as those observed in the 20th

486 century from natural or internal fluctuations.

487

495

496

497

498    **References:**

499    Ahmed, M. and the PAGES 2k Consortium: Continental-scale temperature variability during the last
500       two millennia, Nature Geosci., 6, 339–346, doi:10.1038/ngeo1797, 2013.

501    Årthun, M., Eldevik, T., Smedsrud, L.H., Skagseth, Ø., Ingvaldsen, R.B.: Quantifying the influence of
502       Atlantic heat on Barents Sea ice variability and retreat, J. Climate, 25, 4736-4743,
503       doi:10.1175/JCLI-D-11-00466.1, 2012.

504    Beitsch, A., Jungclaus, J.H., and Zanchettin, D.: Patterns of decadal-scale Arctic warming events in
505       simulated climate. Clim. Dynam.,  43, 1773-1789, doi:10.1007/s00382-013-2004-5, 2014.

506    Bengtsson, L., Semenov, V.A., and Johannessen, O.M.: The early twentieth-century warming in the
507       Arctic – a possible explanation. J. Climate, 18, 4045-4057, doi:10.1175/1520-0442, 2004.

508    Bjerknes, J.: Atlantic air-sea interaction, Adv. Geophys., 10, 1-82, 1964.

509    Booth, B.B.B., Dunstone, N.J., Halloran, P.R., Andrews, T., and Bellouin, N.: Aerosols implicated as a
510       prime driver of twentieth century North Atlantic climate variability, Nature, 484, 228-232,
511       doi:10.1038/nature10946, 2012.

512    Born, A., Stocker, T.F., Raible, C.C., and Levermann, A.: Is the Atlantic subpolar gyre bistable in
513       comprehensive climate models? Clim. Dynam, 40, 2993-3007, doi:10.1007/s00382-012-1525-7,
514       2013a.

515    Born, A., Stocker, T.F., and Sandø, A.B.: Coupling of eastern and western subpolar North Atlantic: salt
516       transport in the Irminger Current, Ocean Sci. Discuss., 10, 555-579, 2013b.

517    Bothe, O., Jungclaus, J.H., and Zanchettin, D.: Consistency of the multi-model CMIP5/PMIP3
518       ensemble, Clim. Past, 9, 2471-2487, doi:10.5194/cp-9-2471-2013201, 2013.

519    Carton, J.A., and Giese, B.S.: A reanalysis of ocean climate using Simple Ocean Data Assimilation
520       (SODA). Mon. Weather Rev., 136, 2999-3017, doi: 10.1175/2007MWR1978.1, 2008.

521    Crowley, T.J., and Unterman, M.B.: Technical details concerning development of a 1200 yr proxy
522       index for global volcanism, Earth Syst. Sci. Data, 5, 187-197, doi:10.5194/essd-5-187-2013, 2013.

523    Cunningham, L., Austin, W.E.N., Knudsen, K.L., Eiriksson, J., Scourse, J.D., Wanamaker, A.D. Jr., Butler,
524       P.G., Cage, A.G., Richter, T. Husum, K., Hald, M., Andersson, C., Zorita, E., Linderholm, H.W.,
525       Gunnarson, B.E., Sicre, M.-A., Sejruo, H.P., Jiang, H., and Wilson, R.: Reconstructions of surface
526       ocean conditions from the northeast Atlantic and Nordic Seas during the last millennium. The
527       Holocene, 23, 921-935, doi:10.1177/0959683613479677, 2013.

528    Drijfhout, S.S., and Hazeleger, W.: Changes in MOC and gyre-induced Atlantic Ocean heat transport,
529       Geophys Res. Lett., 33, L07707, doi:10.1029/2006GL025807, 2006.

530    Drijfhout, S., van Oldenborgh, G.J., and Cimatoribus, A.: Is a decline of AMOC causing the warming
531       hole above the North Atlantic in observed and modeled warming patterns? J. Climate, 25, 8373-
532       8379, doi:10.1175/JCLI-D-12-00490.1, 2012.

533    Dylmer, C.V., Giradeau, J., Eynaud, F., Husum, K., De Vernal, A.: Northward advection of Atlantic
534       water in the eastern Nordic Seas, Clim. Past, 9, 1505-1518, doi:10.5194/cp-9-1505-2013, 2013.

535    Eden, C., and Jung, T.: North Atlantic interdecadal variability: oceanic response to the North Atlantic
536       Oscillation (1865-1997), J. Climate, 14, 676-691, 2001.

537    Fernández-Donado, L., González-Rouco, J.F., Raible, C.C., Ammann, C.M., Barriopedro, D.,  García-
538       Bustamante, E., Jungclaus, J.H., Lorenz, S.J., Luterbacher, J., Phipps,  S.J., Servonnat, J.,
539       Swingedouw, D.,  Tett, S.F.B., Wagner, S., Yiou, P.,  and Zorita, E.: Large-scale temperature

540 response to external forcing in simulations and reconstructions of the last millennium, Clim.Past,
541 9, 393-421, doi:10.5194/cp-9-393-2013, 2013.

542 Giorgetta, M. A., Jungclaus, J. H., Reick, C. H., Legutke, S., Brovkin, V., Crueger, T., Esch, M., Fieg, K.,
543 Glushak, K., Gayler, V., Haak, H., Hollweg, H.-D., Ilyina, T., Kinne, S., Kornblueh, L., Matei, D.,
544 Mauritsen, T., Mikolajewicz, U., Mueller, W. A., Notz, D., Raddatz, T., Rast, S., Redler, R., Roeckner,
545 E., Schmidt, H., Schnur, R., Segschneider, J., Six, K., Stockhause, M., Wegner, J., Widmann, H.,
546 Wieners, K.-H., Claussen, M., Marotzke, J., and Stevens, B.: Climate and carbon cycle changes from
547 1850 to 2100 in MPI-ESM simulations for the Coupled Model Intercomparison Project phase 5, J.
548 Adv. Model Earth Syst., 5, 1–26, doi:10.1002/jame.20038, 2013.

549 Greatbatch, R., Fanning, A., Goulding, A., and Levitus, S.: A diagnosis of interpentadal circulation
550 changes in the North Atlantic, J. Geophys. Res., 96, 22,009-22,023, 1991.

551 Häkkinen, S., and Rhines, P.B.: Shifting surface currents in the northern North Atlantic, J. Geophys.
552 Res., 114, C04005, doi:10.1029/2008JC004883, 2009.

553 Hald, M., Salomonsen, G.R., Husum, K., and Wilson, L.J.: A 2000 year record of Atlantic Water
554 temperature variability from Malangen Fjord, northeastern North Atlantic, The Holocene, 21,
555 1049-1059, doi:10.1177/095968361140057, 2011.

556 Hall, I.R., Boessenkool, K.P., Barker, S., McCave, N., and Elderfield, H.: Surface and deep ocean
557 coupling in the subpolar North Atlantic during the last 230 years. Paleoceanography, 25, PA2101,
558 doi:10.1029/2009PA001886, 2010.

559 Hátún, H., Sandø, A.B., Drange, H., Hansen, B., and Valdimarsson, H.: Influence of the Atlantic
560 subpolar gyre on the thermohaline circulation. Science, 309, 1841-1844,
561 doi:10.1126/science1114777, 2005.

562 Jungclaus, J.H., Macrander, A., and Käse, R.H.: Modelling the overflow across the Greenland-Scotland
563 Ridge, in: Arctic-subarctic ocean fluxes, edited by Dickson, R.R., Meincke, J., and Rhines, P.,
564 Springer, Dordrecht, 527-549, 2008.

565 Jungclaus, J.H., Lorenz, S.J., Timmreck, C., Reick, C.H., Brovkin, V., Six, K., Segschneider, J., Giorgetta,
566 M.A., Crowley, T.J., Pongratz, J., Krivova, N.A., Vieira, L.E., Solanki, S.K., Klocke, D., Botzet, M.,
567 Esch, M., Gayler, V., Haak, H., Raddatz, T.J., Roeckner, E., Schnur, R., Widmann, H., Claussen, M.,
568 Stevens, B., and Marotzke, J.: Climate and carbon-cycle variability over the last millennium, Clim.
569 Past, 6, 723-737, doi:10.5194/cp-6-723-2010, 2010.

570 Jungclaus J.H., and Koenigk T.: Low-frequency variability of the Arctic climate: the role of oceanic and
571 atmospheric heat transport variations. Clim. Dynam., 34, 265-279, doi:10.1007/s00382-009-0569-
572 9, 2010.

573 Jungclaus, J.H., Fischer, N., Haak, H., Lohmann, K., Marotzke, J., Matei, D., Mikolajewicz, U., Notz, D.,
574 and von Storch, J.-S.: Characteristics of the ocean simulations in the Max Planck Institute Ocean
575 Model (MPIOM) the ocean component of the MPI-Earth system model, J. Adv. Model Earth Syst.,
576 5, 422-446, doi:10.1002/jame.20023, 2013.

577 Kaufman, D.S., Schneider, D.P., McKay, N.P., Ammann, C.M., Bradley, R.S., Briffa, K.R., Miller, G,H.,
578 Otto-Bliesner, B.L., Overpeck, J.T., Vinther, B.M., and Arctic Lakes 2K project members: Recent
579 warming reverses long-term Arctic cooling. Science, 325, 1236-1239,
580 doi:10.1126/science.1173983, 2009.

581 Keith, D.W.: Meridional energy transport: uncertainty in zonal means. Tellus, 47A, 30-44, 1995.

582 Kim, H., and S.-I. An: On the subarctic North Atlantic cooling due to global warming. Theor. Appl.
583 Climatol., 114, 1-19, doi:10.1007/s00704-012-0805-9, 2012.

584  Kinnard, C., Zdanowicz, C.M., Fisher, D.A., Isaksson, E., De Vernal, A., and Thompson, L.G.:
585      Reconstructed changes in Arctic sea ice over the last 1,450 years. Nature, 479, 509-513,
586      doi:10.1038/nature10581, 2011.

587  Koenigk, T., Brodeau, L.: Ocean heat transport into the Arctic in the twentieth and twenty-first
588      century in EC-Earth, Clim. Dynam., 43, 3101-3120, doi:10.1007/s00382-013-1821-x ,2014.

589  Latif, M., Böning, C., Willebrand, J., Biastoch, A., Dengg, J., Keenlyside, N., Schweckendiek, U., and
590      Madec, G.: Is the Thermohaline Circulation Changing?. J. Climate, 19, 4631–4637, doi:
591      http://dx.doi.org/10.1175/JCLI3876.1, 2006.

592  Levermann, A., and Born, A.: Bistability of the Atlantic subpolar gyre in a coarse-resolution climate
593      model. Geophys. Res. Lett., 34, L24605, doi:10.1029/2007GL031732, 2007.

594  Lohmann, K., Jungclaus, J.H., Matei, D., Mignot, J., Menary, M., Langehaug, H.R., Ba, J., Gao, Y.,
595      Otterå, O.H., Park, W., and Lorenz, S.: The role of subpolar deep water formation and Nordic Seas
596      overflows in simulated multidecadal variability of the Atlantic meridional overturning circulation.
597      Ocean Sci., 10, 227-241, doi:10.5194/os-10-227-2014, 2014.

598  Lozier, M.S.: Deconstructing the Conveyor Belt, Science, 328, 1507-1511,
599      doi:10.1126/science.1189250 ,2010.

600  Lozier, M.S., Roussenov, V., Reed, M.S.C., and Williams, R.G.: Opposing decadal changes for the
601      North Atlantic meridional overturning circulation. Nature Geosci., 3, 728-734,
602      doi:10.1038/NGEO947, 2010.

603  Mahlstein I., and Knutti, R.: Ocean heat transport as a cause for model uncertainty in projected Arctic
604      warming, J. Climate, 24, 1451-1460, doi:10.1175/JCLI3713.1 ,2011.

605  Marsland, S.J., Haak, H., Jungclaus, J.H., Latif, M., and Roeske, F.: The Max- Planck- Institute global
606      ocean/sea-ice model with orthogonal curvilinear coordinates, Ocean Modelling, 5, 91-127, 2003.

607  Miettinen, A., Divine, D., Koç, N., Godtliebsen, F., and Hall, I.R.: Multicentennial variability of the sea
608      surface temperature gradient across the subpolar North Atlantic over the last 2.8kyr, J. Climate,
609      25, 4205-4219, doi:10.1175/JCLI-D-11-00581.1, 2012.

610  Mjell, T.L., Ninnemann, H.F., H.F. Kleiven, and Hall, I.R.: Multidecadal changes in Iceland-Scotland
611      overflow water vigor over the last 600 years and its relation to climate. Under review: Geophys.
612      Res. Lett., 2014.

613  Müller, W.A., Matei, D., Bersch, M., Jungclaus, J.H., Haak, H., Lohmann, K., Compo, G.P.,
614      Sardeshmukh, P.D., and Marotzke, J.: A 20th century reanalysis-forced ocean model to reconstruct
615      the North Atlantic climate variations during the 1920s. Clim. Dynam., in press: doi:
616      10.1007/s000382-014-2267-5, 2014.

617  Østerhus, S., and Gammelsrød, T.: The abyss of the Nordic Seas is warming. J. Climate, 12, 3297-3304,
618      1999.

619  Pavlov, A., Tverberg, V., Ivanov, B., Nilsen, F., Falk-Petersen, S., and Granskog, M.: Warming of
620      Atlantic Water in two west Spitsbergen fjords over the last century (1912-2009). Polar Research,
621      32, 11206, doi:10.3402/polar.v32i0.11206, 2013.

622  Polyakov, I.V., Alekseev, G.V., Timokhov, L.A., Bhatt, U.S., Colony, R.L., Simmons, H.L., Walsh, D.,
623      Walsh, J.E., Zakharov, V.F.: Variability of the Intermediate Atlantic Water of the Arctic Ocean over
624      the last 100 years, J. Climate, 17, 4485-4497, 2004.

625  Polyakov, I.V., Alexeev, V.A., Bhatt, U.S., Polyakova, E.I., and Zhang, X.: North Atlantic warming:
626      patterns of long-term trend and multidecadal variability. Clim. Dynam., 34, 439-457,
627      doi:10.1007/s00382-008-0522-3, 2010.

628 Pongratz J., Reick, C.H., Raddatz, T., and Claussen, M.: A reconstruction of global agricultural areas
629     and land cover for the last millennium, Glob. Biogeochem. Cycles, 22, GB3018,
630     doi:10.1029/2007GB003153, 2008.

631 Rayner, N.A., Brohan, P., Parker, D.E., Folland, C.K., Kennedy, J.J., Vanicek, M., Ansell, T.J., and Tett,
632     S.F.B.: Improved analyses of changes and uncertainties in sea surface temperature measured in
633     situ since the mid nineteenth century: the HadSST2 data set. J. Climate, 19, 446-469,
634     doi:10.1175/jcli3637.1.

635 Reverdin, G.: North Atlantic Subpolar Gyre Surface Variability (1895-2009). J. Climate, 23, 4571-4584,
636     doi: 10.1175/2010JCLI3493.1.

637 Saenko, O.A., Fyfe, J.C., and England, M.H.: On the response of the oceanic wind-driven circulation to
638     atmospheric $CO_2$ increase. Clim. Dynam., 25, 415-426, doi:10.1007/s00382-005-0032-5, 2005.

639 Schauer, U., Beszynnka-Möller, A., Walczowski, W., Fahrbach, E., Piechura, J., and Hansen, E.
640     Variations of measured heat flow through Fram Strait between 1997 and 2006, in: Arctic-subarctic
641     ocean fluxes, edited by Dickson, R.R., Meincke, J. and Rhines, P., Springer, Dordrecht, 65-85, 2008.

642 Schmidt, G.A., Jungclaus, J.H., Ammann, C.M., Bard, E., Braconnot, P., Crowley, T.J., Delaygue, G.,
643     Joos, F., Krivova, N.A., Muscheler, R., Otto-Bliesner, B.L., Pongratz, J., Shindell, D.T., Solanki, S.K.,
644     Steinhilber, F., Vieira, L.E.A.: Climate forcing reconstructions for use in PMIP simulations of the
645     last millennium (v.1.0), Geosci. Model Dev., 4, 33-45, doi:10.5194/gmd-4-33-2011 ,2011.

646 Serreze, M.C., Barnett, A.P., Slater, A.G., Steele, M., Zhang, J., and Trenberth, K. E.: The large-scale
647     energy budget of the Arctic. J. Geophys. Res., 112, D11122, doi:10.1029/2006JD008230, 2007.

648 Sedláček, J., and Mysak, L.A.: 2009: A model study of the Little Ice Age and beyond: changes in ocean
649     heat content, hydrography and circulation since 1500. Clim. Dyn., 33, 461-475, 2009.

650 Shaffrey, L., and Sutton, R.: Bjerknes compensation and the decadal variability of the energy
651     transports in a coupled climate model, J. Clim., 19, 1167-1448, doi:10.1175/JCLI3652.1, 2006.

652 Shi, F., Yang, B., Ljungqvist, F.C., and Yang, F.: Multi-proxy reconstruction of Arctic summer
653     temperatures over the past 1400 years, Clim. Res., 54, 113-128, doi:10.3354/cr01112, 2012.

654 Skagseth, in: Arctic-subarctic ocean fluxes, edited by Dickson, R.R., Meincke, J., and Rhines, P.,
655     Springer, Dordrecht, 45-64, 2008.

656 Smith, T.M., and Reynolds, R.W.: Improved extended reconstruction of SST (1854-1997). J. Climate,
657     17, 2466-2477, doi: 10.1175/1520-0442(2004)017<2466:IEROS>2.0.CO;2, 2004.

658 Spielhagen, R.F., Wagner, K., Sørensen, S.A., Zamelczyk, K., Kandiano, E., Budeus, G., Husum, K.,
659     Marchitto, T.M., and Hald, M.: Enhanced modern heat transfer to the Arctic by warm Atlantic
660     Water, Science 331 450-453, doi:10.1126/science.1197397, 2011.

661 Stevens, B., Giorgetta, M., Esch, M., Mauritsen, T., Crueger, T., Rast, S., Salzmann, M., Schmidt, H.,
662     Bader, J., Block, K., Brokopf, R., Fast, I., Kinne, S., Kornblueh, L., Lohmann, U., Pincus, R., Reichler,
663     T., and Roeckner, E.: Atmophereric component of the MPI-M Earth system Model: Echam6, J.
664     Adv. Model Earth Syst., 5, 146-172, doi:10.1002/jame.20015, 2013.

665 Vieira, L.E.A., Solanki, S.K., Krivova, N.A., and Usoskin, I.: Evolution of the solar irradiance during the
666     Holcene, Astron. Astroph., 531, A6, doi:10.1051/0004-6361/201015843, 2011.

667 Wang, Y.-M., Lean, J.L., Sheeley Jr., N.R.: Modeling the Sun's magnetic field and irradiance since
668     1713, Astrophys. J., 625, 522-538, doi:10.1086/4296889, 2005.

669 Werner, K., Spielhagen, R.F., Bauch, D., Hass, H.C., Kandiano, E., and Zamelcyk, K.: Atlantic water
670     advection to the eastern Fram Strait – multiproxy evidence for late Holocene variability,
671     Paleogeography, Paleoclimatology, Paleoecology, 308, 264-276, doi:10.1016/j.paleo.2011.05.030,
672     2011.

673    Zanchettin, D., Timmreck, C., Graf, H.-F.  Rubino, A., Lorenz, S., Lohmann, K., Krüger, K., and
674       Jungclaus, J.H.: Bi-decadal variability excited in the coupled ocean-atmosphere system by strong
675       tropical volcanic eruptions, Clim. Dynam., 39, 419-444, doi:10.1007/s00382-011-1167-1, 2012.

676    Zanchettin, D., Timmreck, C., Bothe, O., Lorenz, S.J., Hegerl, G. Graf, H.-F., Luterbacher, J., and
677       Jungclaus, J.H.: Background conditions influence the decadal climate response to strong volcanic
678       eruptions. *J. Geophys. Res. Atmos.*, 118, doi:10.1002/jgrd50229, 2013.

679    Zhang, R., Delworth, T.L., Sutton, R., Hodson, D.L.R., Dixon, K.W., Held, I.M., Kushnir, Y., Marshall, J.,
680       Ming, Y., Msadek, R., Robson, J., Rosati, A.J., Ting, M.F., and Vecci, G.: Have aerosols caused the
681       observed Atlantic multidecadal variability? J. Atm. Sci., 70, 1135-1144, doi:10.1175/JAS-D-12-
682       0331.11, 2013.

683
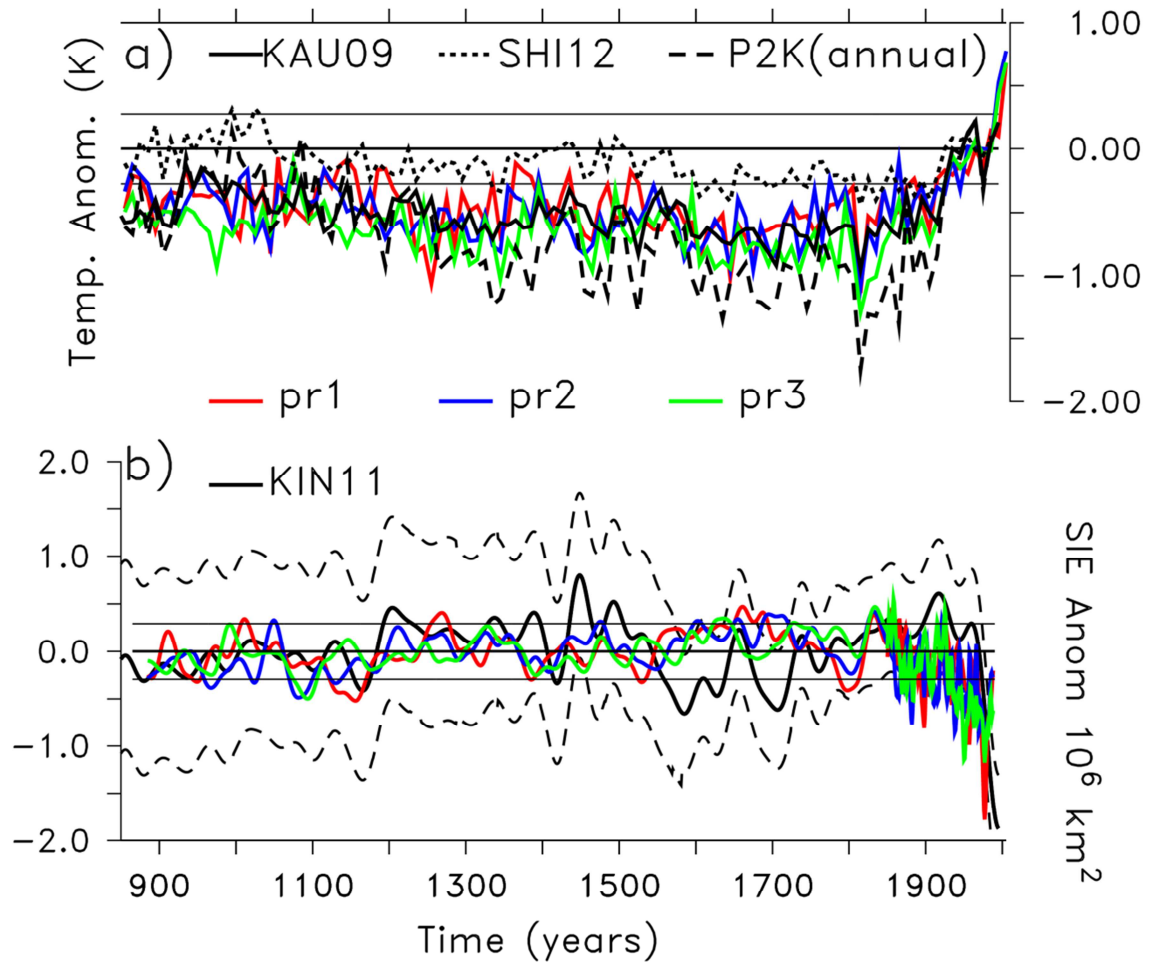
**Figures**



**Figure 1:** Simulated time series (colored lines for experiments pr1, pr2, pr3) of high northern latitude climate variables in comparison with reconstructions (black lines): **a)** 10-year averages of Arctic summer (JJA) surface air temperatures as anomalies w.r.t. the 1960-1990 mean. Summer temperature reconstructions are from: (solid black) Kaufman et al. (2009), and (dotted black) Shi et al. (2012). The PAGES2K reconstruction representing annual temperatures is also shown (dashed black). **b)** late-summer (August) sea-ice extent (in 106 km2) as anomalies w.r.t. the pre-industrial mean in comparison with the reconstruction by Kinnard et al. (2011): The thick black line denotes the 40-year smoothed reconstruction, the dashed black lines their 95% confidence interval; for the simulations, a 41-yr running mean was applied for pre-industrial millennium and a 5-yr running mean for 1850-2005 to better display 20th century variability. Thin horizontal lines bracketing the zero line in **a)** and **b)** indicate the respective 2σ-ranges derived from the 1000yr-long PiCtrl experiment.
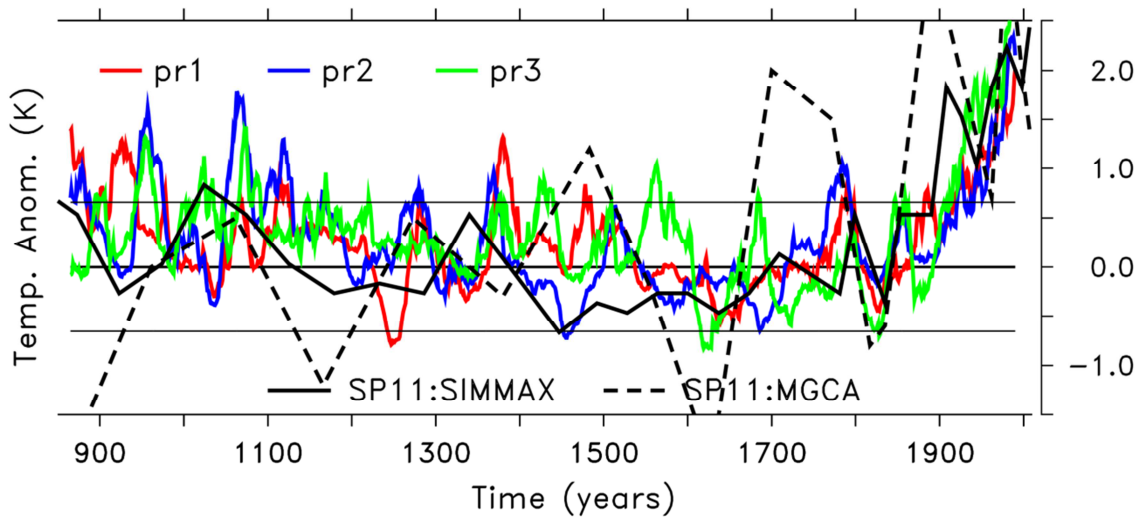
**Figure 2:** Simulated time series (colored lines for experiments pr1, pr2, pr3) of Arctic Atlantic Water temperature anomalies w.r.t. the pre-industrial mean in Fram Strait (78°N, 50m depth) in comparison with the reconstruction by Spielhagen et al. (2011) obtained by the (solid black) SIMMAX, and (dashed black) Mg/Ca methods, respectively. The thin horizontal lines bracketing the zero line indicate the respective 2σ-ranges derived from the 1000yr-long PiCtrl experiment.

707



708
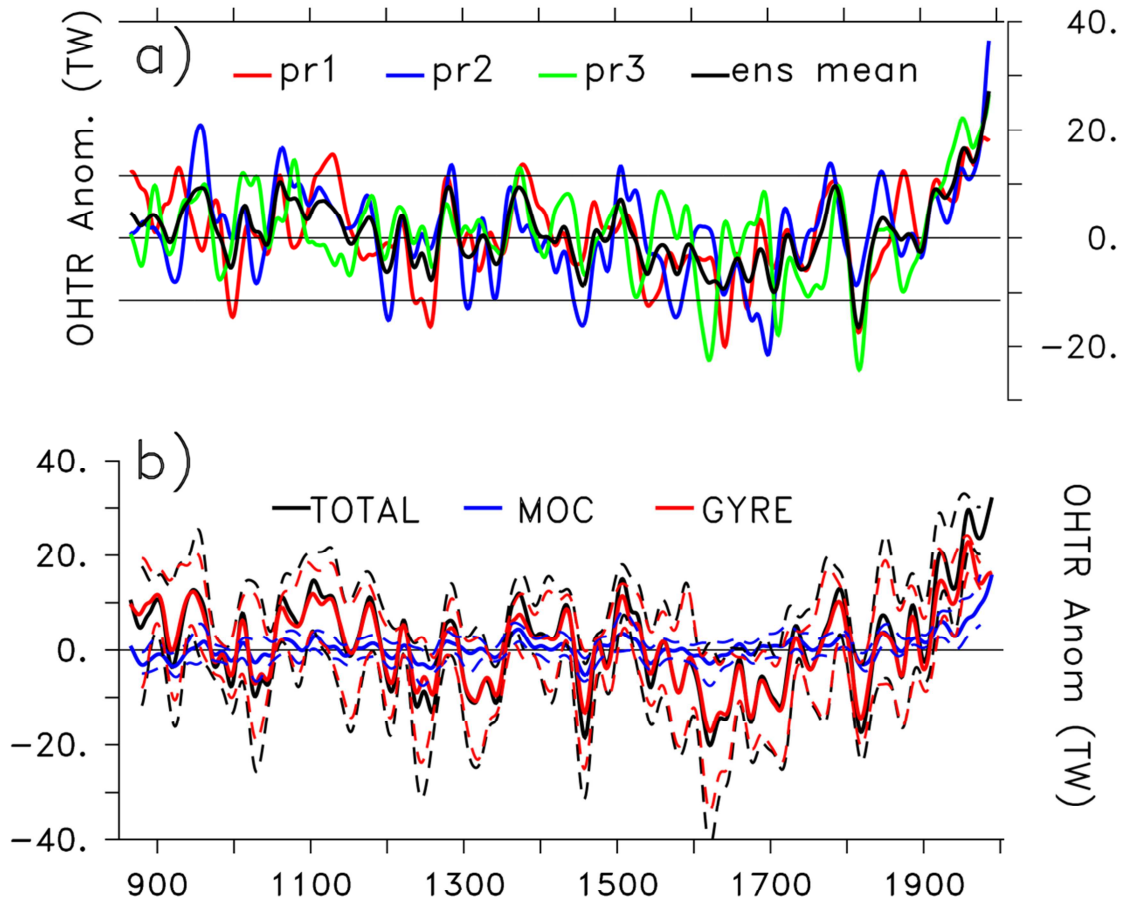
**Figure 3: a)** Simulated ocean heat transport (OHTR) to the Arctic (combined OHTR through Fram
Strait and Barents Sea Opening) as anomalies w.r.t. the pre-industrial mean; colored lines indicate
individual simulations pr1, pr2 and pr3, and the solid black line is the ensemble mean, thin horizontal
lines bracketing the zero line indicate the respective 2σ-ranges derived from the 1000yr-long PiCtrl
experiment. **b)** Total OHTR (black lines, TOHTR) averaged over 60-65°N, subdivided into gyre-related
OHTR (red, GOHTR), and overturning-circulation-related OHTR (blue, MOHTR). Thick lines represent
the ensemble means and the dashed lines the respective ensemble ranges. All time-series were
smoothed by a 31-yr running mean. Units are TW (1 TW = $10^{12}$ Watt).

717

718

719
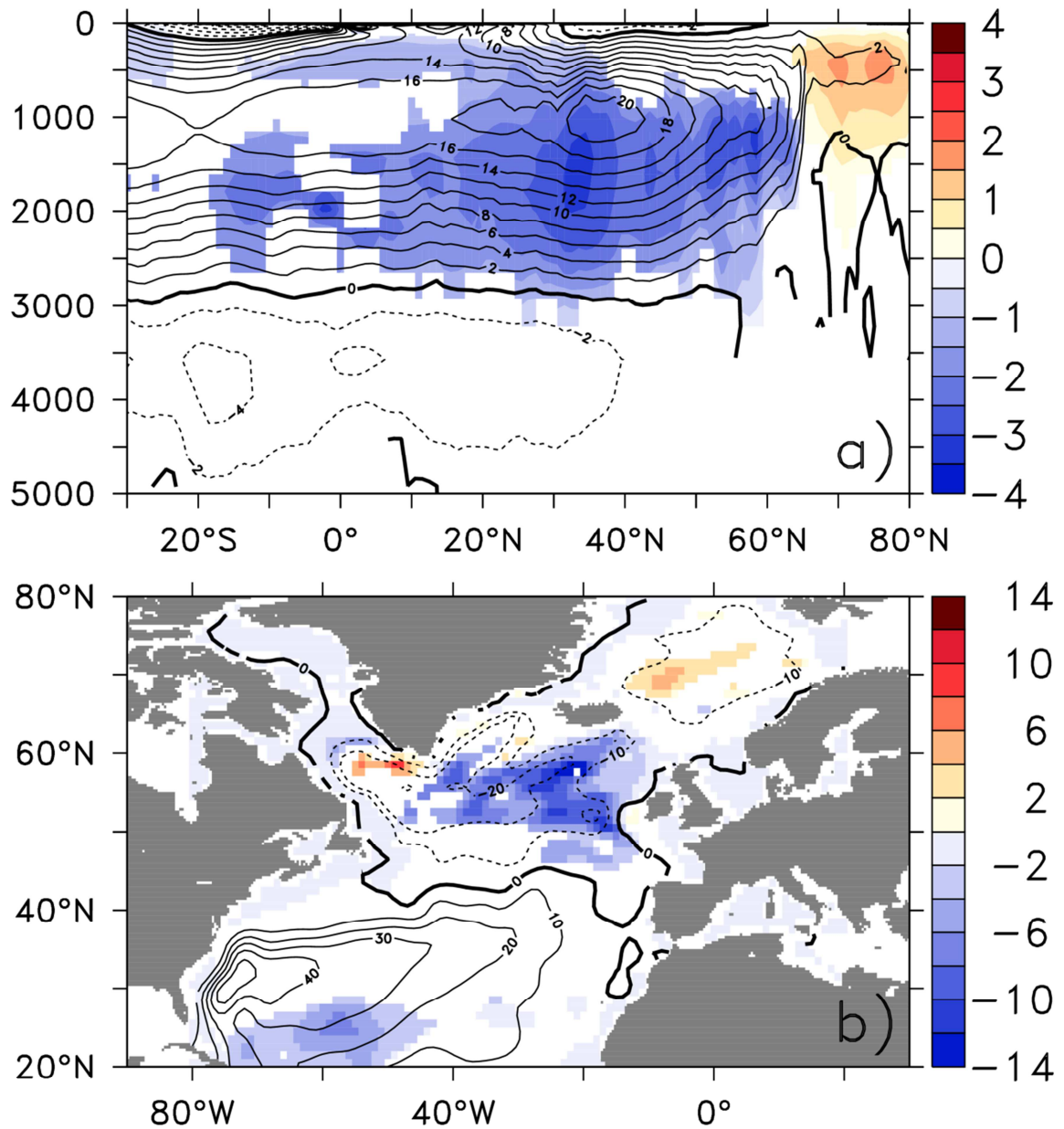
**Figure 4:** Simulated 20th century linear trends (1905-2005) in the pr2 simulation (color shading) of a) meridional overturning circulation, and b) barotropic stream function in the North Atlantic. Units are Sverdrups per 100 yrs (1 Sv = $10^6$m$^3$s$^{-1}$). Contour lines (contour intervals 2 SV for overturning and 10 Sv for barotropic stream function) describe the pre-industrial mean state. In both panels, only anomalies are shown that exceed the 5-95%-tile range of centennial trends derived from the PiCtrl simulations.

731



732

733
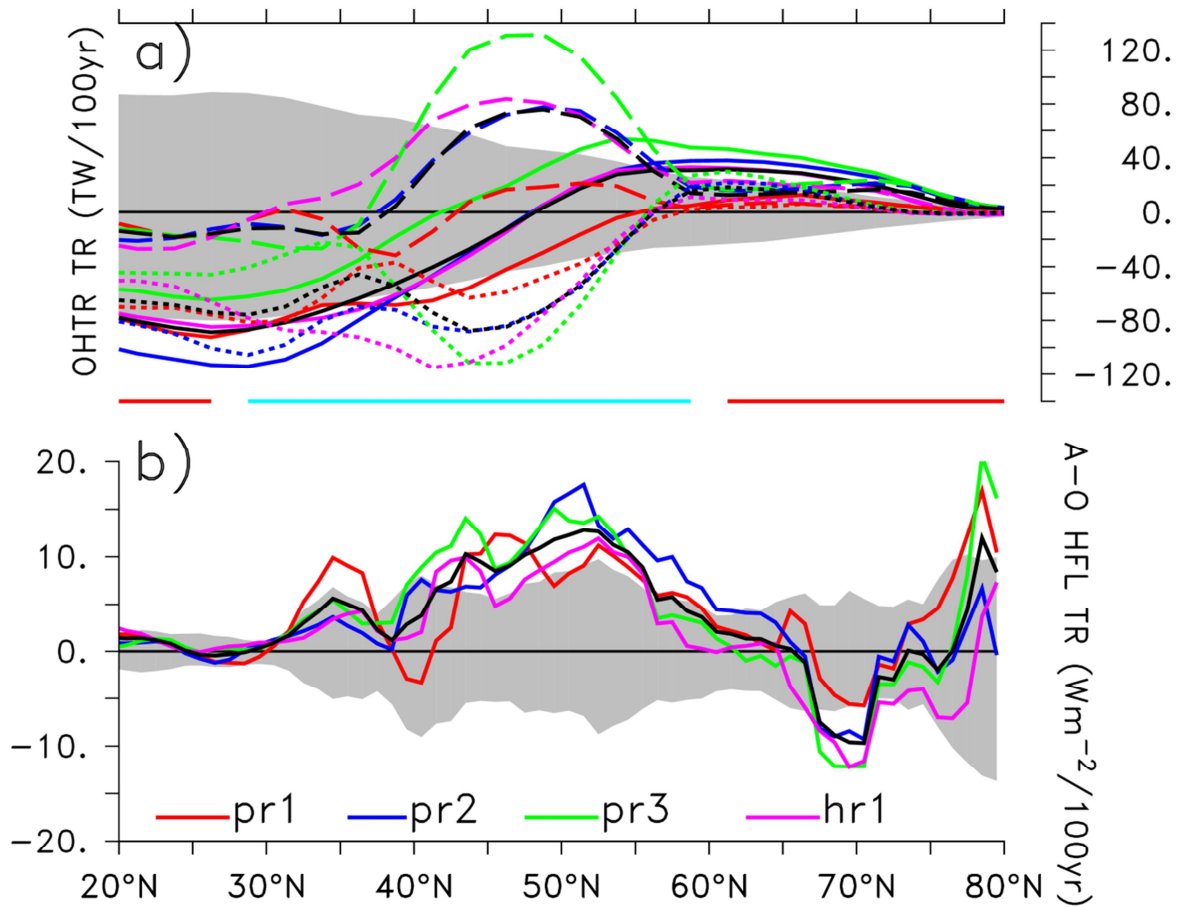
**Figure 5:** Simulated 20th century linear trends (1905-2005) as zonal averages over the Atlantic basin (experiments pr1, pr2, pr3, and hr1 as indicated by colored lines, black lines indicate ensemble means): **(a)** (solid lines) TOHTR, (dashed lines) GOHTR, and (dotted lines) MOHTR. Light-blue and red horizontal lines at the bottom of the plot indicate regions, where the ensemble-mean TOHTR divergence is positive (cooling by lateral advection: light-blue) or negative (warming by lateral advection: red). **(b)** atmosphere-ocean heat fluxes. Positive values indicate increased heat transfer from the atmosphere to the ocean or cooling of the atmosphere by the ocean. Colored lines are individual simulations and the black line is the ensemble mean. In **(a)** and **(b)**, the grey-shaded regions indicate the 5-95%-tile ranges of centennial trends in the unperturbed PiCtrl experiment.

743
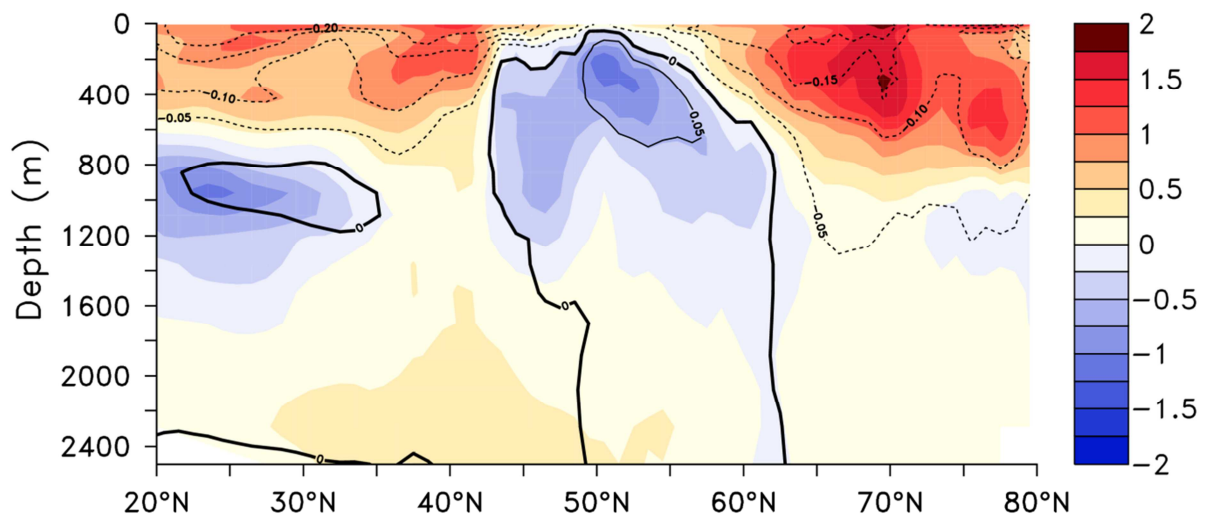
744

745

746

747



748

749

750 **Figure 6:** Simulated 20$^{th}$ century linear trends (1905-2005) as zonal averages over the Atlantic basin
751 for potential temperature (color shading) and density (contours, contour interval 0.05 kgm$^{-3}$) trends
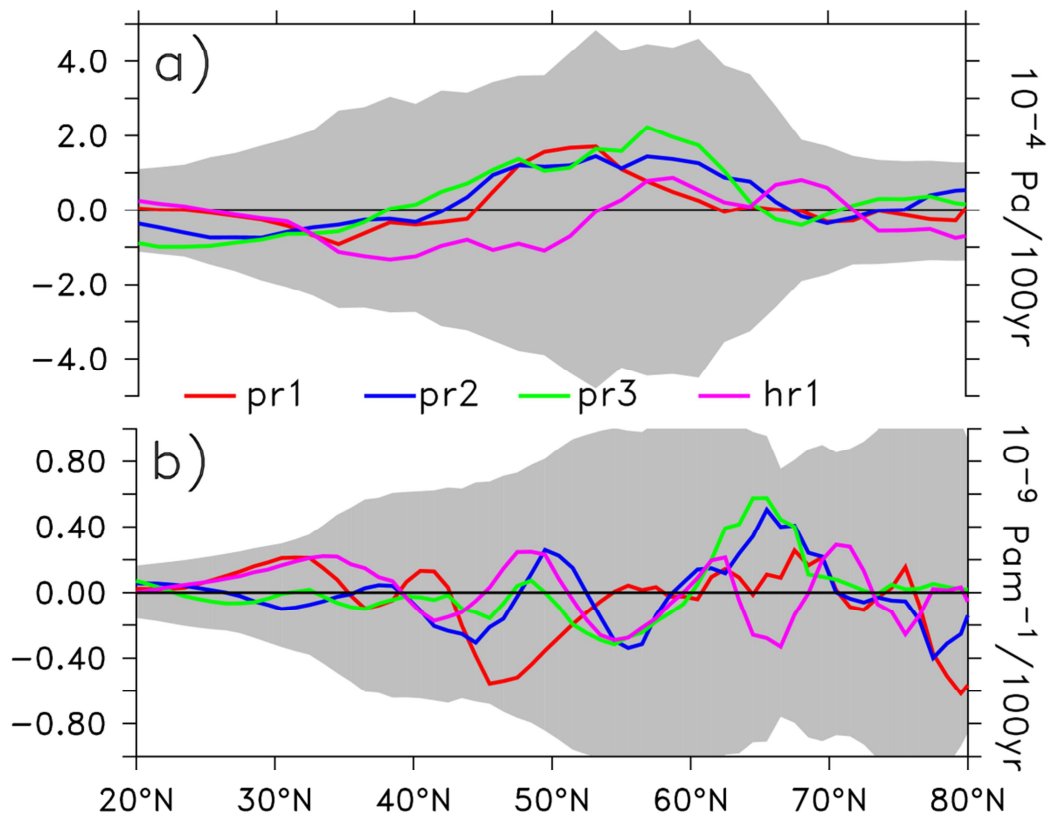752 from the pr2 experiment.

753

754

755

756

757

758

759



**Figure 7:** Simulated (experiments pr1, pr2, pr3, and hr1) 20th century linear trends (1905-2005) as zonal averages over the Atlantic basin of **(a)** wind stress (units $10^{-2}$ Pa/100 yrs)and **(b)** wind stress curl (in $10^{-9}$ Pa m$^{-1}$/100yrs). Colored lines denote the experiments pr1, pr2, pr3, and hr1 and the grey-shaded regions bracketing the zero line show the 5-95%-tile range of centennial trends in the unperturbed PiCtrl experiment.

760

761

767

768

769
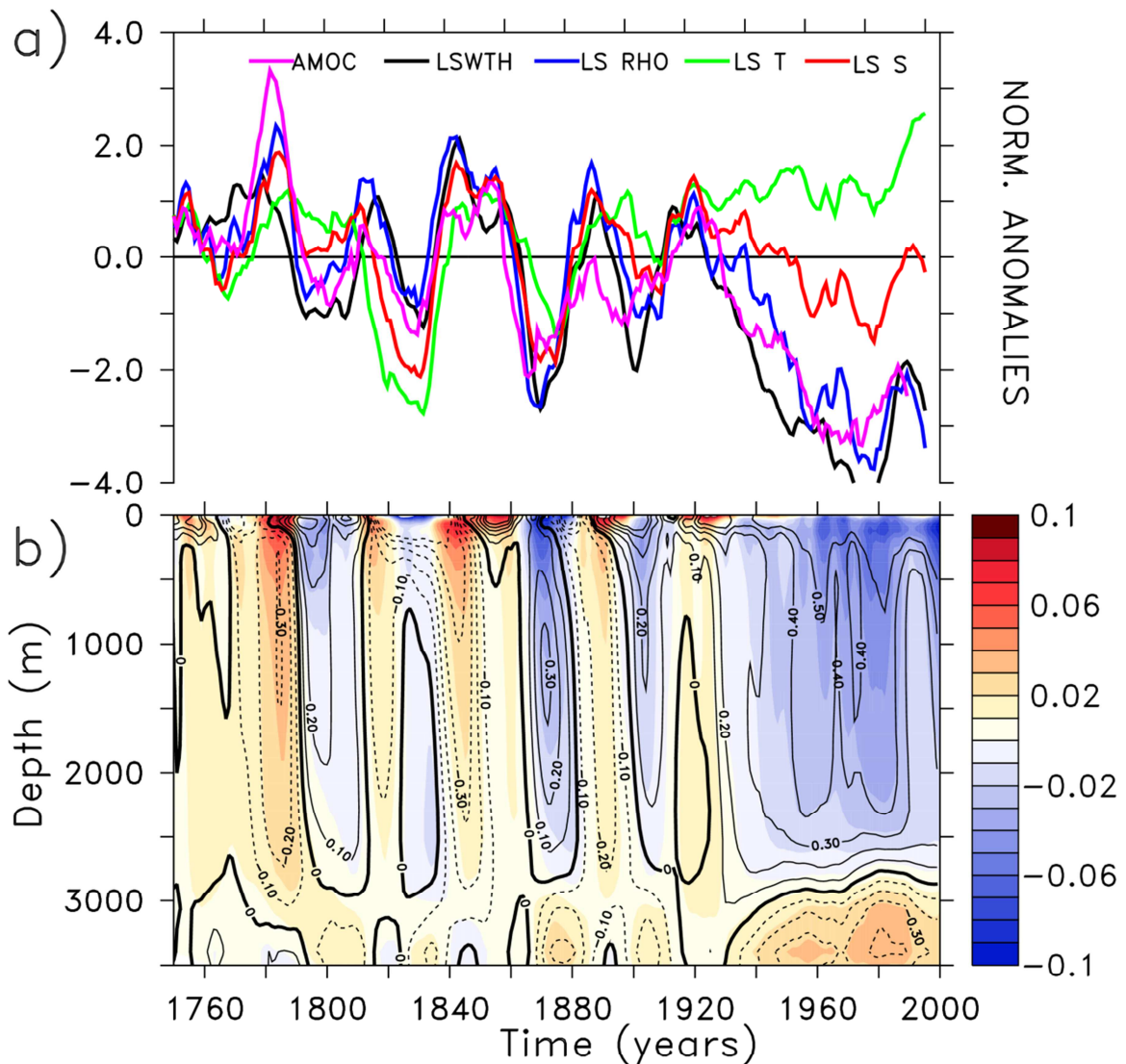
**Figure 8: (a)** Evolution of the Labrador Sea Water thickness, AMOC stream function at 30N and 1500m depth (displayed here with a 10-year time lag), and surface water mass properties in the region, where convection takes place in the Labrador Sea: Density (LS RHO), temperature (LS T), and salinity (LS S). All time-series are smoothed using an 11-yr running mean and are shown as normalized anomalies w.r.t. the pre-industrial means. **(b)** Evolution of potential density (color shading) and potential temperature (contours, contour intervals 0.05 K) as function of depth and time for the Labrador Sea in the pr2 simulation. A 11-yr running mean was applied to the data.

780
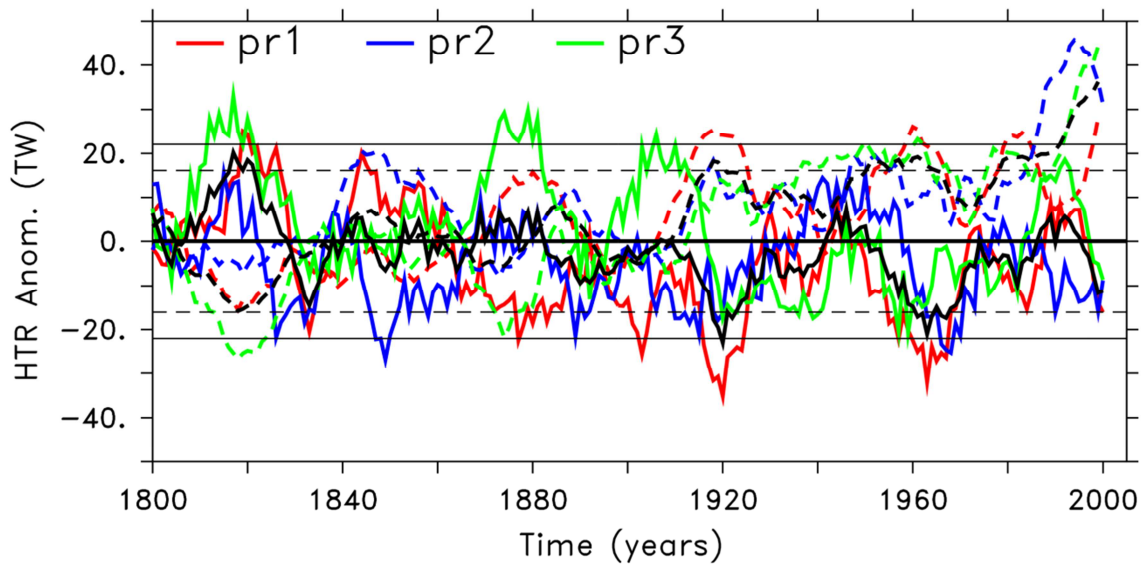
**Figure 9:** Time series of simulated (solid lines) atmospheric heat transports (AHTR) and (dashed lines) TOHTR at 70°N as anomalies w.r.t. the pre-industrial mean (colored lines for experiments pr1, pr2, pr3;  time series shown as black dashed and solid lines denote the respective ensemble means). The horizontal black lines bracketing the zero lines are the respective 2-σ ranges derived from the PiCtrl experiment. An 11-yr running mean was applied to all data sets.

786